C. R. Palevol 14 (2015) 139–145

Contents lists available at ScienceDirect

Comptes Rendus Palevol

www.sciencedirect.com

Human palaeontology and prehistory

The age-related maturational pattern of the human subarcuate fossa (petromastoid canal). Preliminary results from the application of a new three-dimensional analytical approach

Caractéristiques de maturation de la fossa subarcuata (canal pétromastoïdien) chez l'homme en fonction de l'âge. Résultats préliminaires à partir de l'application d'une nouvelle approche analytique tridimensionnelle

Delphine Carayon[a,b,*], Frédéric Vaysse[a,c], Paul Tramini[b], Jean Dumoncel[a], Rémi Esclassan[a,c]

[a] *Laboratoire Anthropobiologie moléculaire et imagerie de synthèse (AMIS), UMR 5288 CNRS – Université de Toulouse Paul-Sabatier, 37, allée Jules-Guesde, 31000 Toulouse, France*
[b] *UFR d'Odontologie Montpellier-I, 545, avenue du Professeur-Jean-Louis-Viala, 34080 Montpellier, France*
[c] *UFR d'Odontologie Toulouse-III, avenue des Maraîchers, 31062 Toulouse, France*

ARTICLE INFO

Article history:
Received 9 June 2014
Accepted after revision 30 October 2014
Available online 13 January 2015

Handled by Roberto Macchiarelli

Keywords:
Human temporal bone
Bony labyrinth
Subarcuate fossa
Development
Micro-CT scanner
3D image analysis

ABSTRACT

The subarcuate fossa, or petromastoid canal, is a hypostotic feature of the temporal bone used for assessing the age at death of immature individuals. The present study uses the high-resolution micro-CT record of 20 extant human infant and juvenile temporal bones to more precisely assess the age-related maturational pattern of this bony structure. In the perspective of the application of our analytical protocol to the study of the hominid fossil record, the main goals of this contribution are to extend the amount and to improve the quality of the linear and volumetric information on the human subarcuate fossa by the application of new 3D imaging techniques.

Mots clés :
Os temporal humain
Labyrinthe osseux

RÉSUMÉ

La fossa subarcuata ou canal petromastoïdien, est un caractère hypostotique de l'os temporal utilisé pour estimer l'âge au décès des individus immatures. La présente étude utilise

* Corresponding author at: Laboratoire Anthropobiologie moléculaire et imagerie de synthèse (AMIS), UMR 5288 CNRS – Université de Toulouse Paul-Sabatier, 37, allée Jules-Guesde, 31000 Toulouse, France.
E-mail address: delphinedom.carayon@orange.fr (D. Carayon).

http://dx.doi.org/10.1016/j.crpv.2014.10.004
1631-0683/

Fossa subarcuata
Développement
Scanner micro-CT
Analyse d'image 3D

les images haute résolution micro-CT de 20 os temporaux humains immatures et juvéniles, afin d'estimer plus précisément la maturation en lien avec l'âge de cette structure osseuse. En vue d'appliquer notre protocole analytique à l'étude du registre fossile hominidé, les principaux objectifs de ce travail sont d'améliorer la quantité et la qualité des informations volumétriques et linéaires de la fossa subarcuata, par l'application de nouvelles techniques d'imagerie 3D.

1. Introduction

In paleobiological and palaeoanthropological research, interpreting the maturational patterns of anatomical regions is of great interest for the assessment of the accurate age at death of immature individuals, notably in the case of isolated fossil specimens. Among the intracranial features, the subarcuate fossa (SF), or petromastoid canal (CPM), has been recognized as a valuable hypostotic trait of the temporal bone to assess developmental age in human and nonhuman extant and fossil primates (e.g., Braga et al., 2013; Coqueugniot et al., 2004; Gannon et al., 1988; Jeffery et al., 2008; Spoor and Leakey, 1996; Weaver, 1979). This anatomical structure (hereinafter referred to as SF, i.e., subarcuate fossa) is located in the bony labyrinth, which includes the sense organs of hearing in the cochlea and of balance in the vestibule and the semicircular canals. It is circumscribed by the three semicircular canals and is more precisely located on the posterior surface of the petrous pyramid, superolateral to the internal acoustic meatus (Jeffery and Spoor, 2004, 2006). The SF is present in the prenatal stages of all primate species but, in some taxa, it may be obliterated after birth (Spoor and Leakey, 1996).

Among humans, the particularity of SF depends on its postnatal ossification, making an osseous depression termed the petromastoid canal (CPM). This extends posterolaterally through the arch of the anterior canal toward the mastoid antrum. At birth, the bony labyrinth has reached its adult size and will remain invariant. In contrast, the FS will gradually decrease during the first 2 years, reaching its final size in c. 3 years (Dutailly et al., 2007).

Rapid advances in computer technology offer nowadays the opportunity of high quality two- (2-) and three-dimensional (3D) reconstructions and provide increasingly precise imaging techniques for noninvasively investigating inner fossil structures (e.g., Bayle et al., 2011; Clément and Geffard-Kuriyama, 2010; Weber and Bookstein, 2011). By using biometric references with a more precise imaging technique and at a higher resolution than medical computed tomography (Maret et al., 2010, 2014), in this preliminary study we investigate the age-related maturational pattern of the human subarcuate fossa. More precisely, the objectives of this contribution are to improve previous methods applied to the analysis of the human fossil record (e.g., Coqueugniot et al., 2004) and to test a new 3D imaging approach allowing a more subtle quantitative assessment of this bony structure.

2. Materials and methods

2.1. Sample and scanning procedures

The investigated sample consists of 20 crania of immature modern individuals (*H. sapiens*) selected from the reference anatomical collection of the Faculty of Medicine of Strasbourg. Details are given in Table 1. Both sex (11 males and 9 females) and age (ranging from new-born to 10 years) were known for all individuals (Rampont, 1994).

The temporal region of each specimen was scanned at the Institute for Space Medicine and Physiology (MEDES) of Toulouse with a Scanco Medical™ X-Treme micro-CT scanner by using the following parameters: 60 kV, 1 mA, 41 μm isotropic resolution. Image data were interpolated to form isometric voxels. The resulting voxel size from which the volumetric measurements were taken was $0.041 \times 0.041 \times 0.041$ mm. Data were exported in DICOM format before being converted to TIFF format for subsequent segmentation of the bony labyrinth and the subarcuate fossa. The software used for 3D visualization of the internal structures of the petrous pyramid and for linear and volumetric measurements was Amira 5.0® (Mercury Computer System®).

2.2. Measurements

The height and width of the SF opening are spatially associated with the arc height and width of the anterior semicircular canal (Jeffery and Spoor, 2006). Based on the micro-CT record, the SF was quantitatively assessed by means of linear and volumetric measurements.

2.2.1. Linear measurements

Two-dimensional measurements of the subarcuate fossa were performed on micro-CT slices. Its degree of obliteration was measured using the method elaborated by Coqueugniot et al. (2004). The SF maximum width (*f* wid) was measured along a segment joining the two lumens of the anterior semicircular canal (whose width corresponds in this study to the variable *c* wid) in a plane parallel to the arc of the lateral semicircular canal. The linear measurements were taken to the nearest hundredth of a millimetre and the SF width (*f* wid) was expressed as a percentage of the arc width of the anterior semicircular canal (*c* wid) in the same slice (ratio = *f* wid/*c* wid). A first series of measurements was taken (*f* wid 1/*c* wid 1). To test intra-observer reproducibility, we carried out a second series of measurements (*f* wid 2/*c* wid 2) after an interval of 1 week. Left and right sides were averaged for each individual.

Table 1
Composition of the investigated sample ($n = 20$) and individual volumetric (in mm^3) and ratio values (in %) of the subarcuate fossa (provided for each side, if available). Besides the indication 'neonate', ages are given in months (m) or years (y).
Tableau 1
Nature de l'échantillon étudié ($n = 20$) et valeurs individuelles du volume (mm^3) et du ratio (en %) de la fossa subarcuata (droite et gauche, si possible). Outre les indications « nouveau-né », les âges sont donnés en mois (m) ou années (a).

Individual	Calendar Age	Sex	Fossa Volume mm^3		Fossa Subarcuata %				
			Right	Left	Right	Left	Mean	Published 2004	Published 2013
Embr 249	Neonate	M	15.7	14.3	30.9	41.3	36		36
Embr 323	Neonate	M	3.8	8.3	30.3	51.8	41		38
Embr 168	Neonate	M	22.2	25.1	55.5	36.6	46		49
Embr583	2 m.	F	6.1	3.9	22.4	17	20		20
Embr 308	2 m. 15 d.	F	18.3	39.7	44.1	42.8	43	34	44
Embr 385	5 m.	F	2.3	1.5	19.7	10.6	15		16
Embr 277	6 m.	M		1.5		27.7			
Embr215	7 m.	M	7.5	2.8	21.3	20.3	21	9	21
Embr 513	7 m.	F	1.6		15.5			14	
Embr 576	7 m.	F	12.5		25.1			23	
Embr 388	1 y.	M	8	7.6	16.2	22.3	19	16	20
Embr 479	1 y.3 m.	M	9.9	3.5	25.1	25.3	25	19	27
Embr 281	1 y. 10 m.	F	3	2.2	13.7	23.6	37	16	21
Embr 384	2 y. 1 m.	F	4.6	7.2	30.6	31	31		29
Embr 205	3 y.	M	4.7	1.3	18.4	17.9	18		16
Embr 473	3 y. 4 m.	M	2.6	4.7	23	27.8	25	0	25
Embr 121	5 y.	F	2.9	2.2	24.9	14	19		19
Embr 212	5 y.	F	3.2	2.1	23	14.7	19		24
Embr 136	6 y.	M	1.6	4.1	8.2	11.8	10		11
Embr 179	10 y.	M	0.7	0.7	5.9	8.1	7		0

M: male; F: female.

Correlation and regression analyses were performed with the mean values (between left and right sides). No significant differences were found when values (L and R sides) were analysed all together or individually with the Wilcoxon matched-pairs signed-rank test (*pc* wid = 0.17, *pf* wid = 0.95 and *pf* vol = 0.85). The ratios are given in Table 1 (see also Table 2).

2.2.2. Volumetric measurements

One of the aims of this preliminary study was to accurately estimate SF volume (*f* vol, in mm^3) in order to determine the degree of obliteration of the SF by using a new 3D approach in addition to the conventional bivariate analysis. This because, compared to the volume of the labyrinth (l vol), the SF is not a clearly circumscribed and easily quantifiable entity. However, the two reference planes used here to define it were systematically taken perpendicular to the main axis of the fossa and were defined by two anatomical features:

- the external opening of the fossa to the vestibular aqueduct;
- the three openings for the cranial nerve branches (Fig. 1).

Besides a first observer (DC), the position of these two reference planes was validated by a second, independent observer (RE). Volumetric data are given in Tables 1 and 2.

Table 2
Descriptive statistics of the variables considered in this study distinctly for the right and left side.
Tableau 2
Statistiques descriptives des variables étudiées de manière distincte pour les côtés droit et gauche.

	Right ($n = 19$)		Left ($n = 17$)	
	Mean	SD	Mean	SD
f wid	1.59	0.79	1.57	0.76
c wid	6.65	0.28	6.53	0.46
ratio	23.88	11.58	24.14	11.68
f vol	6.91	6.16	6.99	9.88
l vol	170.49	27.32	171.44	28.81

f wid: subarcuate fossa maximum width (mm); *c* wid: anterior semicircular canal width (mm); ratio: *f* wid/*c* wid (%); *f* vol: subarcuate fossa volume (mm^3); *l* vol: labyrinth volume (mm^3).

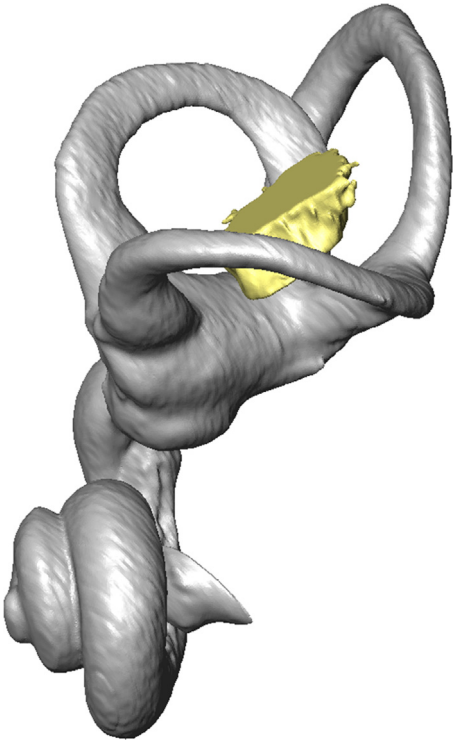

Fig. 1. (Color online.) Micro-CT-based 3D rendering of a modern human labyrinth (right side, in frontal view) with indication of the subarcuate fossa circumscribed by two reference planes (see the text for explanations).
Fig. 1. (Couleur en ligne.) Image micro-CT d'un labyrinthe osseux d'un humain moderne après traitement 3D (côté droit en vue frontale) avec présence de la fossa subarcuata circonscrite par les deux plans de références (voir le texte pour les explications).

2.3. Statistical analyses

Correlations between variables were assessed using the Spearman Test with the Bonferroni correction. All pairwise correlations were performed in order to validate the consistency of the results. The Mann-Whitney test was used in order to compare each parameter between different groups. A Principal Component Analysis (PCA) was performed to analyse the relationships between fossa size and age, providing a graph according to the first two components. The statistical software was Stata v13®. Hypotheses were rejected at *P*-values ≤ 0.05.

3. Results

The PCA under constraints (PCA with instrumental variables) was used as a means to understand the relationships between a set of covariates (in this preliminary study, fossa size) and asymmetric, often dependent variables (age) Baty et al., 2006; Bougeard et al., 2007. Results show that, in the extant human sample used in this study, the volume of the subarcuate fossa (*f* vol), the *SF* width (*f* wid), and the *f* wid/*c* wid fossa ratio (ratio) were inversely correlated with age according to the first component, while the volume of the labyrinth (*l* vol) and the width of the anterior semicircular canal (*c* wid) were relatively invariant (Fig. 2).

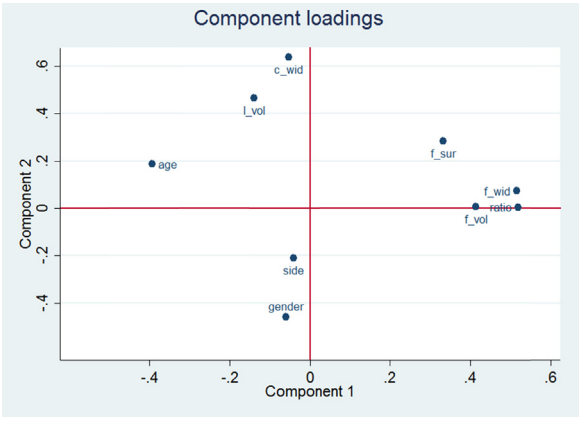

Fig. 2. (Color online.) Component loadings of the Principal Component Analysis. *f* wid: subarcuate fossa maximum width; *c* wid: anterior semicircular canal width; ratio: *f* wid/*c* wid; *f* vol: subarcuate fossa volume; *l* vol: labyrinth volume.
Fig. 2. (Couleur en ligne.) Étude des paramètres par une analyse en composante principale (ACP). *f* wid : largeur maximale de la fossa subarcuata ; *c* wid : largeur du canal semi-circulaire antérieur ; ratio : *f* wid/*c* wid ; *f* vol : volume de la fossa subarcuata ; *l* vol : volume du labyrinthe.

The percentage of variance explained by the first two principal components is 57%. Both correlations between fossa volume and age ($P = 0.007$) and between fossa ratio and age ($P = 0.02$) are significant (Table 3). It is noteworthy that the fossa ratio decreased after birth and its relationship with age could be modelled by linear regression, with a negative slope ($y = -0.2077x + 29.4$, $R^2 = 0.317$).

The relationship between fossa volume and age could also be modelled by linear regression, with a negative slope ($y = -0.1072x + 9.73$, $R^2 = 0.175$). The quality of prediction improved after a log transformation of the variables [age = 44.225–13.206 log (*f* vol)/age = 154.77–42.097 log (ratio)]. R^2 rose from 0.17 to 0.23 (fossa volume) and from 0.32 to 0.46 (ratio). Together with the mean errors (21.7 months for the variable *f* vol and 20.9 months for the ratio *f* wid/*c* wid), estimations of the confidence intervals are shown on Figs. 3 and 4.

The Breusch–Pagan/Cook–Weisberg test for heteroscedasticity was not significant ($P = 0.17$). Accordingly, homoscedasticity was accepted for the residuals of the linear regression (age × fossa volume) (Fig. 5).

Table 3
Analysis of the correlation with age of the variables considered in this study (see Table 2).
Tableau 3
Analyse de la corrélation avec l'âge des variables étudiées (voir Tableau 2).

	Spearman correlation coefficient	*P* value
Log (*f* wid)	−0.58	0.03
Log (*c* wid)	0.23	0.67
Log (ratio)	−0.58	0.02
Log (*f* vol)	−0.55	0.007
Log (l vol)	0.38	0.42

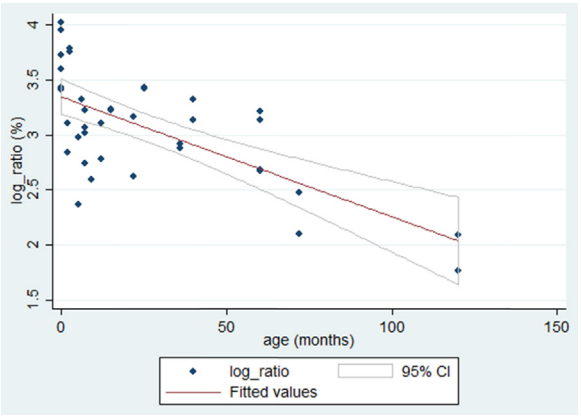

Fig. 3. (Color online.) Linear regression of the subarcuate fossa log ratio (*f* wid/*c* wid) according to age with estimation of the confidence interval.
Fig. 3. (Couleur en ligne.) Régression linéaire du ratio de la fossa subarcuata (*f* wid/*c* wid) en fonction de l'âge avec estimation de l'intervalle de confiance.

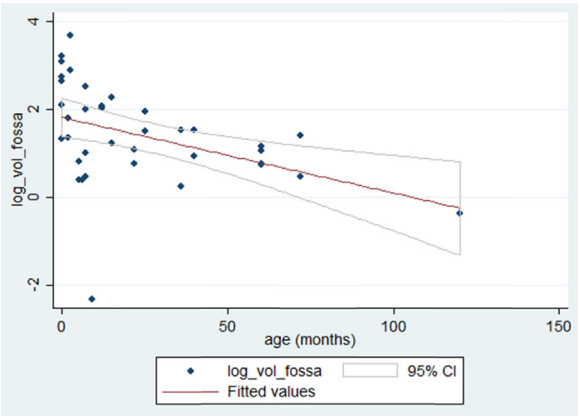

Fig. 4. (Color online.) Linear regression of the subarcuate fossa log volume (*f* vol) according to age with estimation of the confidence interval.
Fig. 4. (Couleur en ligne.) Régression linéaire du volume de la fossa subarcuata (*f* vol) en fonction de l'âge avec estimation de l'intervalle de confiance.

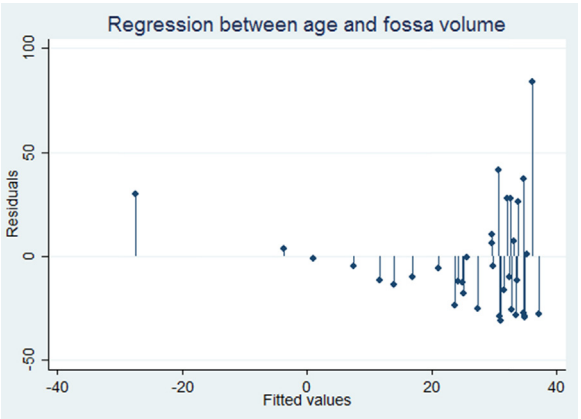

Fig. 5. (Color online.) Regression (residuals analysis) between age and subarcuate fossa volume (*f* vol).
Fig. 5. (Couleur en ligne.) Analyse des résidus entre l'âge et le volume de la fossa subarcuata (*f* vol).

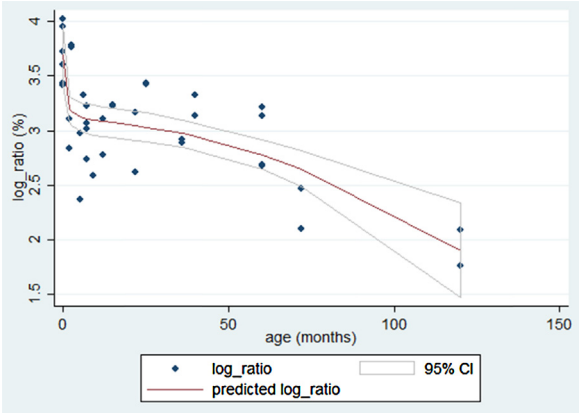

Fig. 6. (Color online.) Fractional polynomial regression of the subarcuate fossa ratio (*f* wid/*c* wid) according to age.
Fig. 6. (Couleur en ligne.) Régression polynomiale du ratio de la fossa subarcuata (*f* wid/*c* wid) en fonction de l'âge.

The relationships between fossa size parameters and age fitted by a fractional polynomial regression with confidence interval are illustrated on Figs. 6 and 7. In both cases, the slope is very steep from the birth to circa 12 months of age, but becomes nearly flat after the first year. At the best of our knowledge, this represents a previously unreported evidence which deserves additional investigation (through a polynomial regression analysis) performed on a larger and specifically selected sample.

4. Discussion and conclusion

A major objective of the present study was to extend the amount and improve the quality of the biometric (linear and volumetric) information currently available on the extant human subarcuate fossa (SF) in the perspective of its application to the analysis of the fossil record. For example, by using medical CT images (0.199-mm pixel size) coupled with linear measurements (SF width relative to the distance across the anterior semicircular canal), Coqueugniot

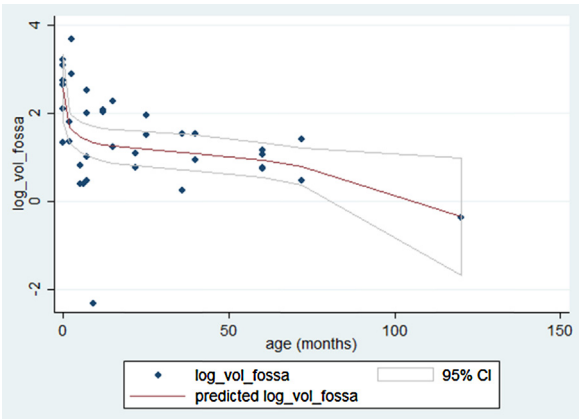

Fig. 7. (Color online.) Fractional polynomial regression of the subarcuate fossa volume (*f* vol) according to age.
Fig. 7. (Couleur en ligne.) Régression polynomiale du volume de la fossa subarcuata (*f* vol) en fonction de l'âge.

et al. (2004) firstly investigated the degree of closure of the SF in order to tentatively constrain the age at death estimate of the Early Pleistocene Indonesian *Homo erectus* child from Mojokerto, Java (contra, see Balzeau et al., 2005), and compared their findings to the available patterns reported for extant humans and *Pan*. More recently, based on the high resolution record (performed at 18.3-μm and 7.4-μm isometric voxel size, respectively) obtained by two industrial and synchrotron micro-CT scanners, Braga et al. (2013) accurately assessed the degree of obliteration and the linear dimensional features of the SF in order to estimate the individual developmental age and taxonomic status of the juvenile hominin specimen KB 6067, an isolated petrous temporal bone from the site of Kromdraai B, Gauteng, South Africa, likely representing *Paranthropus robustus*.

Our preliminary study, which uses both 2D and 3D variables to characterize the developmental patterning of the subarcuate fossa in a modern human reference sample of immature temporal bones, confirms the informative value of such analyses, notably when based on a high resolution micro-CT record, but also reveals a certain degree of fluctuating asymmetry in the *SF* width and volume, and this at all age stages (Table 1). This evidence, while not statistically significant in the sample investigated so far (Wilcoxon matched-pairs signed-rank test: $P = 0.95$ for the FS width; $P = 0.84$ for the ratio; $P = 0.85$ for the volume), nonetheless cautions about the reliability of age at death estimates uniquely relying upon measurements performed on a single petrosal bone and points to the need for extending such primarily methodological work to larger series (Hallgrimsson et al., 2007).

In the literature, there is no methodological consensus about the volumetric assessment of the subarcuate fossa. Accordingly, the second objective of our study was to test a new 3D analytical approach tentatively granting reproducible finer results.

In their pioneering work aimed to estimate the *SF* volume in representatives from 36 mammal genera (mostly primates), Gannon et al. (1988) investigated the disarticulated crania under a dissection microscope. Each specimen was systematically oriented so that the arch of the anterior semicircular canal was set in a horizontal plane. The SF was then filled with an alcoholic solution up to the medial extent of the ostium formed by the anterior semicircular canal. According to this methodology, the *SF* volume in *H. sapiens* was evaluated as equal to zero after birth.

Details about the morphostructural variation and evolutionary history of the temporal bone labyrinthine features in extant and fossil primates, including hominids, became increasingly clear following the extensive application of enhanced 2–3D imaging techniques (Hublin et al., 1996; Spoor, 1993). For example, in a study aimed at evaluating the possible relationships among semicircular canals size, fossa size, and agility in 167 specimens sampling 68 primate taxa, besides 9 raw and 6 derived linear parameters, Jeffery et al. (2008) also tentatively calculated the *SF* volume by outlining the area of interest in a number of medical CT-based transverse slices, and then by summing the pixel areas multiplied by the slice thickness. Accordingly, the volume was estimated as the sum of outlines that followed the internal contours of the SF and, if necessary, capped by a straight line cutting across its endocranial opening. Since, advances in high-resolution scanning and 3D imaging are rapidly disclosing new perspectives in the quantitative characterization of the structural and functional evolutionary changes of the petrous temporal bone (e.g., Braga et al., 2013).

Besides confirming previously reported evidence about the age-related variation of the subarcuate fossa linear measurements in immature human crania, present results also show that the *SF* volume decreases rapidly after birth and that the growth pattern at early ages does not behave linearly. Additional methodological research developed on larger human and nonhuman primate temporal bone samples detailed at high resolution is needed to refine such preliminary results.

Acknowledgements

We thank the two anonymous reviewers for their helpful comments, which improved the manuscript. Pr Roberto Macchiarelli is greatly acknowledged for his contribution to a better understanding of this article. Finally, the authors thank Susan Becker for her help in the translation.

References

Balzeau, A., Grimaud-Hervé, D., Jacob, T., 2005. Internal cranial features of the Mojokerto child fossil (East Java, Indonesia). J. Hum. Evol. 48, 535–553.

Baty, F., Facompré, M., Wiegand, J., Schwager, J., Brutsche, M.H., 2006. Analysis with respect to instrumental variables for the exploration of microarray data structures. BMC Bioinform. 7, 422.

Bayle, P., Bondioli, L., Macchiarelli, R., Mazurier, A., Puymerail, L., Volpato, V., Zanolli, C., 2011. Three-dimensional imaging and quantitative characterization of human fossil remains. Examples from the NESPOS database. In: Macchiarelli, R., Weniger, G.-C. (Eds.), Pleistocene Databases. Acquisition, Storing, Sharing. Wissenschaftliche Schriften des Neanderthal Museums 4, Mettmann, pp. 29–46.

Bougeard, S., Hanafi, M., Qannari, E.L.M., 2007. Acpvi multibloc : application en épidémiologie animale. J. Soc. Fr. Stat. 148, 76–94.

Braga, J., Thackeray, J.F., Dumoncel, J., Descouens, D., Bruxelles, L., Loubes, J.-M., Kahn, J.-L., Stampanoni, M., Bam, L., Hoffman, J., de Beer, F., Spoor, F., 2013. A new partial temporal bone of a hominin from the site of Kromdraai B (South Africa). J. Hum. Evol. 65, 447–456.

Clément, G., Geffard-Kuriyama, D., 2010. Imaging & 3D in Palaeontology and Palaeoanthropology. C.R. Palevol 9, 255–470.

Coqueugniot, H., Hublin, J.-J., Veillon, F., Houet, F., Jacob, T., 2004. Early brain growth in *Homo erectus* and implications for cognitive ability. Nature 431, 299–302.

Dutailly, B., Coquegniot, H., Couture, C., Courtaud, P., Desbarats, P., Gueorguieva, S., Synave, R., 2007. Imagerie médicale et patrimoine anthropologique : vers un contrôle total de la chaîne des traitements dans l'analyse morphométrique tridimensionnelle. Proc. Symp. Virtual Retrospect. Archeovision 3. Éditions Ausonius, Bordeaux, pp. 45–51.

Gannon, P.J., Eden, A.R., Laitman, J.T., 1988. The subarcuata fossa and cerebellum of extant primates: comparative study of a skull-brain interface. Am. J. Phys. Anthropol. 77, 143–164.

Hallgrimsson, B., Lieberman, D.E., Liu, W., Ford-Hutchinson, A.F., Jirik, F.R., 2007. Epigenetic interactions and the structure of phenotypic variation in the cranium. Evol. Dev. 9, 393–401.

Hublin, J.J., Spoor, F., Braun, M., Zooneveld, F., Condemi, S., 1996. A late Neanderthal with Upper Paleolithic artefacts. Nature 381, 224–226.

Jeffery, N., Ryan, T., Spoor, F., 2008. The primate subarcuate fossa and its relationship to the semi-circular canals. Part II: adult interspecific variation. J. Hum. Evol. 55, 326–329.

Jeffery, N., Spoor, F., 2004. Ossification and midline shape changes of the human fetal cranial base. Am. J. Phys. Anthropol. 123, 78–90.

Jeffery, N., Spoor, F., 2006. The primate subarcuate fossa and its relationship to the semicircular canals. Part I: prenatal growth. J. Hum. Evol. 51, 537–549.

Maret, D., Molinier, F., Braga, J., Peters, O.A., Telmon, N., Treil, J., Inglèse, J.M., Cossié, A., Kahn, J.-L., Sixou, M., 2010. Accuracy of 3D reconstructions based on cone beam computed tomography. J. Dent. Res. 89, 1465–1469.

Maret, D., Peters, O.A., Galibourg, A., Dumoncel, J., Esclassan, R., Kahn, J.-L., Sixou, M., Telmon, N., 2014. Comparison of the accuracy of 3-dimensional cone-beam computed tomography and micro-computed tomography reconstructions by using different voxel sizes. J. Endodont. 40, 1321–1326.

Rampont, M., 1994. Les squelettes, os et dents de fœtus, nouveau-nés et enfants du musée anatomique de Strasbourg. Aspects historiques et catalogue. PhD dissertation, Louis Pasteur University, Strasbourg.

Spoor, F., 1993. The Comparative Morphology and Phylogeny of the Human Bony Labyrinth. PhD dissertation, University of Utrecht, Utrecht.

Spoor, F., Leakey, M., 1996. Absence of the subarcuate fossa in cercopithecids. J. Hum. Evol. 31, 569–575.

Weaver, D.S., 1979. Application of the likelihood ratio test to age estimation using the infant and child temporal bone. Am. J. Phys. Anthropol. 50, 263–269.

Weber, G.W., Bookstein, F.L., 2011. Virtual Anthropology. A Guide to a New Interdisciplinary Field. Springer, Wien.